

Electron–hole correlations govern Auger recombination in nanostructures

John P. Philbin^{*,1} & Eran Rabani^{*,1,2,3}

¹*Department of Chemistry, University of California, Berkeley, California 94720, United States*

²*Materials Science Division, Lawrence Berkeley National Laboratory, Berkeley, California 94720, United States*

³*The Sackler Center for Computational Molecular and Materials Science, Tel Aviv University, Tel Aviv, Israel 69978*

The fast nonradiative decay of multiexcitonic states via Auger recombination is a fundamental process affecting a variety of applications based on semiconductor nanostructures. From a theoretical perspective, the description of Auger recombination in confined semiconductor nanostructures is a challenging task due to the large number of valance electrons and exponentially growing number of excited excitonic and biexcitonic states that are coupled by the Coulomb interaction. These challenges have restricted the treatment of Auger recombination to simple, noninteracting electron–hole models. Herein we present a novel approach for calculating Auger recombination lifetimes in confined nanostructures having thousands to tens of thousands of electrons, explicitly including electron–hole interactions. We demonstrate that the inclusion of electron–hole correlations are imperative to capture the correct scaling of the Auger recombination lifetime with the size and shape of the nanostructure. In addition, correlation effects are required to obtain quantitatively accurate lifetimes even for systems smaller than the exciton Bohr radius. Neglecting such correlations can result in lifetimes that are 2 orders of magnitude too long. We establish the utility of the new approach for CdSe quantum dots of varying sizes and for CdSe nanorods of varying diameters and

lengths. Our new approach is the first theoretical method to postdict the experimentally known “universal volume scaling law” for quantum dots and makes novel predictions for the scaling of the Auger recombination lifetimes in nanorods.

The fast nonradiative decay of multiexcitonic states is a central process to many nanocrystal-based applications.^{1,2} This nonradiative decay occurs primarily via Auger recombination (AR) in which one electron-hole pair recombines by transferring its energy to an additional charge carrier (Fig. (1)). In some cases, such as light harvesting devices, AR can limit performance by rapidly quenching the photoluminescence^{1,3-6} and destroying the population inversion required for nanocrystal based lasers,⁷ while in other cases, such as photodetectors,⁸ single photon sources⁹ and even for photocatalysis,¹⁰ it can improve performance by providing a source of hot electrons. Therefore, developing a unified framework to describe AR is important from both fundamental and applied perspectives.

In recent years, much effort has been put into – and much success obtained in – the development of synthetic techniques and principles that result in nanocrystals (NCs) with rationally designed AR lifetimes.² Synthesizing giant NCs offers the simplest and most well-known approach to increase the AR lifetime. This approach works well because the AR lifetime, τ_{AR} , in single-material quantum dots (QDs) obeys the “universal volume scaling law” (i.e., $\tau_{AR,QD} \propto V$ in QDs).^{1,11-13} However, current theories predict a steeper scaling with the QD volume,¹⁴⁻¹⁶ signifying only a partial understanding of the AR process even in spherical, 0D NCs. In addition to controlling the AR lifetime by changing the system size, many reports have found that an intelligent design of core/shell NCs with sharp or gradual interfaces allows for the AR lifetimes in NCs to be tuned.¹⁶⁻²²

The situation is somewhat more confusing for non-spherical NCs.²³⁻³¹ The AR lifetime in 1D nanorod (NR) structures was reported to scale linearly with the length (L) of the NRs (i.e., $\tau_{AR,NR} \propto L$),

but this observation has not been derived from first principles. Recently, it was argued that the AR decay in PbSe NRs has a crossover from cubic to bimolecular scattering as the length of the NR is increased,²⁸ calling into question the monotonic length dependence. Further complications arise from the difficulty to measure precisely the AR lifetimes²⁴ and also to independently control the dimensions of NRs by current synthetic techniques. In fact, it was shown that NRs of equal volume (but differing diameters and lengths) can have AR lifetimes that differ by more than a factor of 2,²⁷ but whether this indicates a deviation from the volume scaling observed in QDs remains an open question.

Nanoplatelet (NPL) structures appear to provide an example of the breakdown of the volume scaling of AR lifetimes. Contradictory results have been reported for the scaling of AR lifetimes with the lateral area (A). She *et al.* showed that the AR lifetimes are independent of A ,²⁹ while recently it was argued to scale linearly with A , attributed to collisions of excitons limited by their spatial diffusion.³¹ The scaling of the AR lifetime as a function of the number of monolayers (ML) was reported to obey a seventh power dependence, $\tau_{\text{AR,NPL}} \propto (\text{ML})^7$, in CdSe NPLs.³¹ This was rationalized by a simple noninteracting effective mass model.³¹

In order to simplify and better understand the size and dimensionality dependence of AR lifetimes in NCs, a unified theoretical framework for calculating AR lifetimes in 0D, 1D and 2D nanostructures must be developed. Such a development has been hampered by various factors, including limitations resulting from the enormous number of excitonic and biexcitonic states in NCs as well as the difficulties in including electron–hole correlation effects. Indeed, previous theoretical works have relied on a non–atomistic model^{14,32} or a noninteracting electron–hole picture, thought to be suitable for strongly confined systems.^{14–17,33,34} However, this approach fails to handle the continuous transition from strong to weak confinement regimes as well as nanostructures that have both strong and weak confinement along

different dimensions (e.g., weakly confined along the NR axis and strongly confined in the others).

In this Letter, we develop a unified approach for calculating AR lifetimes that is applicable to all degrees of confinement. The approach is based on Fermi's golden rule to couple excitonic with biexcitonic states. Electron-hole correlations are explicitly included in the initial biexcitonic states by solving the Bethe-Salpeter equation (BSE) to obtain correlated electron-hole states which are then used to form the initial biexcitonic states. This procedure captures most of the electron-hole correlation as the exciton binding energy is typically an order of magnitude larger than the biexciton binding energy.³⁵ Through a study of CdSe QDs and NRs of varying dimensions, we show that our approach predicts AR lifetimes in quantitative agreement with experiments whereas the noninteracting formalism often overestimates the AR lifetimes by 1 – 2 orders of magnitude. The shorter AR lifetimes are a consequence of electron-hole pair localization which increases the Coulomb coupling and thereby the AR rate in the interacting formalism. By comparing the interacting and noninteracting formalisms (Fig. (1)), we also make evident the importance of including electron-hole correlations for the first theoretical prediction of the observed volume scaling of the AR lifetime in QDs. Interestingly, the transition to the regime where excitonic effects must be included for an accurate AR lifetime calculation occurs at a surprisingly small diameter in CdSe QDs, below the exciton Bohr radius of CdSe. Additionally, we explain the AR lifetime scaling behavior in terms of the scaling of the Coulomb matrix elements and the density of final states in QDs and NRs. The method presented in this Letter is generally applicable to 0D, 1D, 2D and NC heterostructures.

AR involves the coupling of an initial biexcitonic state ($|B\rangle$) of energy E_B to a final excitonic state ($|S\rangle$) of energy E_S via the Coulomb interaction (V). We utilize Fermi's golden rule to calculate the AR lifetime (τ_{AR}) where we average over thermally distributed initial biexcitonic states and sum over all final

decay channels into single excitonic states:

$$\tau_{\text{AR}}^{-1} = \sum_B \frac{e^{-\beta E_B}}{Z_B} \left[\frac{2\pi}{\hbar} \sum_S |\langle B|V|S\rangle|^2 \delta(E_B - E_S) \right]. \quad (1)$$

In the above, the delta function $\delta(E_B - E_S)$ enforces energy conservation between the initial and final states and Z_B is the partition function for biexcitonic states. Note that later when we compare to experimental values, we use a room temperature β for this Boltzmann weighted average, but we do not include temperature fluctuations in our NC configurations.³⁶

A brute force application of equation (1) for nanostructures is prohibitive for several reasons. First, there is currently no tractable electronic structure method for a fully-correlated biexcitonic state and for excitonic states at high energies. Second, the number of initial and final states that satisfy energy conservation increases rapidly with the system size. For these reasons, computational and theoretical studies of AR in confined nanostructures have relied on a noninteracting formalism to describe $|S\rangle$ and $|B\rangle$:^{14-17,32-34}

$$|S\rangle^{(0)} = a_a^\dagger a_i |0\rangle \otimes |\chi_S\rangle \quad (2)$$

$$|B\rangle^{(0)} = a_b^\dagger a_j a_c^\dagger a_k |0\rangle \otimes |\chi_B\rangle, \quad (3)$$

where the superscript “(0)” signifies a noninteracting picture is used. In the above, a_a^\dagger and a_i are electron creation and annihilation operators in quasiparticle state “ a ” and “ i ”, respectively. The indexes a, b, c, \dots refer to the quasiparticle electron (unoccupied) states and i, j, k, \dots refer to quasiparticle hole (occupied) states, with corresponding quasiparticle energies ε_a and ε_i . In equation (3), $|0\rangle$ is the ground state and $|\chi_S\rangle$ and $|\chi_B\rangle$ are the spin parts of the wavefunctions for excitons and biexcitons, respectively. Within the noninteracting formalism, the excitonic and biexcitonic energies are given by $E_S^{(0)} = \varepsilon_a - \varepsilon_i$ and $E_B^{(0)} = \varepsilon_b - \varepsilon_j + \varepsilon_c - \varepsilon_k$, respectively. The AR lifetime takes an explicit form (see the Methods section

for a detailed derivation and discussion of the spin states studied herein) given by:

$$\begin{aligned} \left(\tau_{\text{AR}}^{(0)}\right)^{-1} &= \frac{2\pi}{\hbar Z_B^{(0)}} \sum_{bckj} e^{-\beta(\varepsilon_b - \varepsilon_j + \varepsilon_c - \varepsilon_k)} \sum_a |V_{bacj}|^2 \delta(\varepsilon_b + \varepsilon_c - \varepsilon_j - \varepsilon_a) \\ &+ \frac{2\pi}{\hbar Z_B^{(0)}} \sum_{bckj} e^{-\beta(\varepsilon_b - \varepsilon_j + \varepsilon_c - \varepsilon_k)} \sum_i |V_{ijbk}|^2 \delta(\varepsilon_b - \varepsilon_j - \varepsilon_k + \varepsilon_i). \end{aligned} \quad (4)$$

The first term on the right hand side (rhs) of equation (4) describes the decay of a negative trion of energy $\varepsilon_b + \varepsilon_c - \varepsilon_j$ into an electron of energy ε_a while one of the holes remains a spectator (we refer to this as the “electron channel” and it is shown pictorially on the left side of Fig. 1), and the second term on the rhs of equation (4) describes the decay of a positive trion of energy $\varepsilon_b - \varepsilon_j - \varepsilon_k$ into a hole of energy ε_i while one of the electrons remains a spectator (we refer to this as the “hole channel”). The explicit form of the Coulomb coupling is then given by:

$$V_{rsut} = \iint \frac{\phi_r(\mathbf{r}) \phi_s(\mathbf{r}) \phi_u(\mathbf{r}') \phi_t(\mathbf{r}')}{|\mathbf{r} - \mathbf{r}'|} d^3\mathbf{r} d^3\mathbf{r}', \quad (5)$$

where $\phi_s(\mathbf{r})$ are the quasiparticle states for electrons ($s \in a$) or holes ($s \in i$) and there is no screening – consistent with Ref. 33 and Ref. 37.

As discussed in the introduction, the noninteracting approach is suitable for nanostructures in the very strong confinement regime, where the kinetic energy is large compared to electron–hole interactions. This approach fails, as shown below, for system sizes in the moderate to weak confinement regimes. The inclusion of electron–hole correlations is mainly of significance in the description of the initial biexcitonic states while for the final excitonic states, the noninteracting framework seems suitable even for weakly confined structures, since the final state describes a highly excited electron–hole pair, above their ionization energy. Therefore, we use a noninteracting description for $|S\rangle$ given by equation (2), but include electron–hole correlations in the description of the initial biexcitonic state. Motivated by the work of Refaely–Abramson *et al.*,³⁷ we express the biexcitonic state as two spatially noninteracting but spin–correlated excitons. This is justified since electron–hole correlations are most significant within excitons

as reflected by the larger exciton binding energy compared to that of biexcitons.³⁵ In our interacting approach the biexcitonic states take the form:

$$|B\rangle = \sum_{b,j} \sum_{c,k} c_{b,j}^B c_{c,k}^B a_b^\dagger a_j a_c^\dagger a_k |0\rangle \otimes |\chi_B\rangle, \quad (6)$$

where the coefficients $c_{b,j}^B$ are determined by solving the Bethe–Salpeter equation (BSE),³⁸ as detailed in Ref. 39. The excitonic energy is given by the noninteracting expression, while the biexcitonic energy is now a sum of the exciton energies, each obtained from the BSE. Within the interacting framework, the AR lifetime is given as a sum of electron–dominated (shown pictorially on the right side of Fig. 1) and hole–dominated contributions:

$$\begin{aligned} \tau_{\text{AR}}^{-1} &= \frac{2\pi}{\hbar Z_B} \sum_B e^{-\beta E_B} \sum_{a,i} \left| \sum_{b,c,j} c_{b,i}^B c_{c,j}^B V_{bacj} \right|^2 \delta(E_B - \varepsilon_a + \varepsilon_i) \\ &+ \frac{2\pi}{\hbar Z_B} \sum_B e^{-\beta E_B} \sum_{a,i} \left| \sum_{j,b,k} c_{a,j}^B c_{b,k}^B V_{ijbk} \right|^2 \delta(E_B - \varepsilon_a + \varepsilon_i), \end{aligned} \quad (7)$$

where there are *coherent* sums of the Coulomb matrix elements multiplied with the coefficients that were obtained by diagonalizing the Bethe–Salpeter Hamiltonian matrix. Due to the presence of electron–hole interactions, all particles are involved in the AR process in the interacting formalism. For further details regarding the theory and the derivations of the above equations, please consult the Methods section.

For the implementation of the above frameworks, we chose the semi–empirical pseudopotential method to model the quasiparticle states.^{42–45} And because we only need quasiparticle states in specific energy ranges (near the band–edge for the initial biexcitonic states and those that satisfy energy conservation for the final excitonic states), we utilize the filter–diagonalization technique^{46,47} to obtain only the required electron and hole eigenstates.⁴⁷ Electron–hole correlations were included in the interacting formalism by solving the BSE within the static screening approximation, where the dielectric constant was taken from the work of Wang & Zunger.⁴³

For QDs, we calculated the AR lifetimes for seventeen wurtzite CdSe QDs with diameters ranging from $D_{\text{QD}} = 2R_{\text{QD}} = 1.2 \text{ nm}$ ($\text{Cd}_{20}\text{Se}_{19}$) to $D_{\text{QD}} = 2R_{\text{QD}} = 5.3 \text{ nm}$ ($\text{Cd}_{1358}\text{Se}_{1360}$). For completeness, we also calculated the fundamental and optical gaps for the CdSe QDs, shown in Fig. 2. The difference in the band and optical gap is the exciton binding energy and is in good agreement with previous studies.^{40,41} This suggests that (a) our model is accurate enough to reproduce single- (fundamental gap) and two-particle (optical gap) properties with the simplification of a uniform dielectric screening and (b) that our computational machinery shows mild scaling with the system size, allowing a direct comparison with experiments for realistic NC sizes.

Fig. 3 displays the AR lifetimes obtained by using both the noninteracting (equation (4)) and interacting (equation (7)) formalisms along with experimental^{1,23,24} measurements of the AR lifetimes. It is clear that neglecting electron-hole correlations in the initial biexcitonic state is only reasonable in the very strong confinement limit, where $R_{\text{QD}} \ll a_{\text{B}}$ (where $a_{\text{B}} = 5.6 \text{ nm}$ is the exciton Bohr radius of CdSe).⁴⁸ The noninteracting-based AR lifetimes increase too rapidly as the volume of the QD increases compared to both the interacting formalism and experimentally measured AR lifetimes. Quantitatively, the computed scaling of the AR lifetime by the noninteracting formalism is $\tau_{\text{AR,QD}}^{(0)} \propto V^{1.69}$, which is in contrast to the known volume scaling of the AR lifetime in single material QDs.¹ On the other hand, the volume scaling is accurately captured by the interacting formalism ($\tau_{\text{AR,QD}} \propto V^{0.99}$), and the overall agreement with the experiments is remarkable. Recall that the previous theoretical studies using a noninteracting formalism for the AR lifetime either studied QDs small enough that the noninteracting formalism was able to relatively accurately predict the volume scaling of the AR lifetime³³ or the theories predicted a stronger dependence on the volume ($\propto V^{5/3}$ to V^2).^{14,15}

To understand the origin of the volume scaling of the AR lifetimes for QDs, we start with Fermi's

golden rule and, for simplicity, focus on the rate of decay to hot electrons via the electron channel (similar arguments also hold for the hole channel) at zero temperature ($b = c \equiv \ell = \text{LUMO}$ and $j \equiv h = \text{HOMO}$) in the noninteracting approach:

$$\left(\tau_{\text{AR,e}}^{(0)}\right)^{-1} = \frac{2\pi}{\hbar} \sum_a |V_{\ell a h}|^2 \delta(\varepsilon_\ell + \varepsilon_\ell - \varepsilon_h - \varepsilon_a), \quad (8)$$

where $\varepsilon_\ell + \varepsilon_\ell - \varepsilon_h = 2E_g$ equals two times the fundamental gap, E_g . The scaling of the AR lifetime depends on the scaling of the final density of state and the Coulomb coupling. The former scales linearly with the volume of the NC.^{49,50} Determining the scaling of the latter is more involved. Naively, one would predict it to scale with R_{QD}^{-1} due to the Coulomb potential. However, because the final hot electron state is highly oscillatory, reflecting the high kinetic energy of the hot electron, and the initial biexcitonic state is slowly varying, the leading term that scales as R_{QD}^{-1} vanishes. The next term, which can be obtained by invoking the stationary phase approximation, scales as R_{QD}^{-3} .¹⁴ Altogether, these arguments predict an Auger lifetime that is proportional to the volume: $\tau_{\text{AR,e}}^{-1} \propto |R_{\text{QD}}^{-3}|^2 R_{\text{QD}}^3 \propto R_{\text{QD}}^{-3}$. Similar arguments hold for the scaling of the Auger lifetime in the interacting formalism.

We find, as predicted, that the density of hot electrons and holes scales linearly with the volume of the NCs (top panel, Fig. 4) in both formalisms. However, the scaling of the average Coulomb coupling squared shows significant deviations from the expected V^{-2} stationary phase result in the noninteracting formalism ($\propto V^{-2.74}$), while in the interacting formalism it scales as expected, $\propto V^{-1.99}$. These different scalings can be rationalized by a more localized electron–hole wavefunction in the interacting case, due to the screened Coulomb electron–hole attraction term in the BSE, leading to more overlap with the wavefunction of the hot electron.

Surprisingly, the noninteracting formalism shows pronounced deviations from the interacting formalism for CdSe QDs with diameters as small as ~ 2.5 nm, much smaller than the exciton Bohr radius

($a_B = 5.6$ nm for CdSe).⁴⁸ This was a rather surprising result as all QDs studied here have $R_{\text{QD}} < a_B$, where electron–hole interactions are rather small compared to the confinement kinetic energy (see inset in Fig. 2).

The deviations in AR lifetimes predicted by the two formalisms are even larger for CdSe NRs. In Fig. 5 we show the calculated and measured^{23–25} AR lifetimes for a series of CdSe NRs of different volumes. It is immediately evident that the noninteracting formalism is quantitatively incorrect for all NRs studied. The noninteracting–based AR lifetimes are also too long by approximately 1 – 2 orders of magnitude! This result arises from an underestimation of the Coulomb coupling due to the electron–hole wavefunctions being delocalized over the entire NR in the noninteracting formalism; there is no electron–hole attraction to localize the electron–hole pair to form a bound Wannier exciton in the noninteracting formalism. In contrast, the interacting formalism predicts the scaling (nearly linearly with volume) as well as the magnitude of the AR lifetimes quite accurately in comparison with the experimental results depicted by the solid blue squares.²³ Based on the results reported for spherical QDs, this is to be expected and further signifies the importance of electron–hole correlations in the AR process in confined nanostructures.

Interestingly, more recent experimental measurements show nearly no volume effect on the AR lifetimes in CdSe NRs (striped blue square),²⁴ however, the same authors reported on the inconsistencies between transient absorption and time–resolved photoluminescence measurements (for the largest system studied, the two measurements differ by a factor of ≈ 3). Similar inconsistencies for NRs were reported for the reverse process, by which a hot exciton decays into a biexcitonic state by impact excitation, leading to multiexciton generation (MEG). Preliminary measurements reported a notable volume dependence of the impact excitation rate,^{51,52} while more recent theoretical work,⁵³ followed by experimental

validation,²⁷ argued that impact excitation rates are volume independent. This suggests that different experimental setups (synthesis and optical measurements) may lead to different scaling behavior. A similar reasoning may also explain the discrepancy between the two sets of experimental results on AR lifetimes shown in Fig. 5. However, more experimental work is needed to fully understand the diversity of experimental outcomes, in particular, given that our new theoretical predictions are consistent with one set of measurements but not the other.

Returning to the AR lifetime scaling with volume in NRs, the noninteracting formalism behaves as $\tau_{\text{AR,NR}}^{(0)} \propto V^{2.02}$. This is expected based on the scaling of the Coulomb matrix elements with the diameter and length of the NR,⁵³ but is in contrast to the scaling observed both experimentally²³ and theoretically using the interacting formalism. Thus, including electron–hole correlations is needed for both a quantitatively and qualitatively accurate description of the AR lifetime calculation in NRs. Intuitively, this result makes sense due to both the lack of confinement along the NR axis and the large electron–hole binding energy in CdSe NRs (~ 200 meV)⁴⁸ contributing to making the noninteracting carrier approximation invalid in NRs.

As mentioned above, it is experimentally difficult to independently control the NR diameter and length; however, it is trivial to do computationally, so we analyzed the AR lifetime scaling separately for the NR diameter and length. We found that the AR lifetime scales approximately *quadratically–cubically* with the length of the NR in the noninteracting formalism, while it scales nearly *linearly* in the interacting formalism (Fig. 6), in agreement with previous experimental measurements.^{23,26–28,30} However, the scaling with the length of the NR depends slightly on the diameter. We also observed an approximate D^3 scaling in the interacting formalism, which still awaits experimental validation.

Our finding that the noninteracting formalism is inaccurate for NRs whereas the interacting formal-

ism is accurate further corroborates previous kinetic models and experiments that argued that the total AR rate in NRs increases quadratically with the number of excitons, $n (k_{\text{AR}}(n) \propto n(n-1)/2)$.^{10,25,28,54} In other words, kinetic models of AR in NRs should model AR as a bimolecular collision of two excitons; in opposition to the combinatorial scaling of $n^2(n-1)/2$ if modeling AR as a three particle collision between free, noninteracting electrons and holes. Overall, these results on CdSe NRs add to the body of work that electrons and holes form bound 1D Wannier excitons in 1D systems such as semiconductor NRs and carbon nanotubes.⁵⁵⁻⁵⁸

In conclusion, the interacting approach developed here for calculating AR lifetimes in NCs provides a framework that is able to predict quantitatively accurate AR lifetimes in both QDs and NRs. Our interacting formalism is the first to postdict the experimentally observed linear volume dependence of the AR lifetime in QDs as well as the correct scaling of the AR lifetimes in NRs with respect to the length and volume. This result was rationalized by noting that the matrix elements in AR lifetime calculations involve a product of the initial electron and hole states; thus, taking into account electron-hole correlations will have a large impact in regimes where the confinement energy is comparable or smaller than the exciton binding energy. Electron-hole correlations result in a localization of the pair, thereby, increasing the Coulomb coupling between the initial and final states. This is especially true in NRs where the lack of confinement along the NR axis makes the electron-hole attraction even more important. The resulting localization of the electron-hole pair leads to dramatic decreases in the AR lifetimes, as large as 2 orders of magnitude, when including such correlations.

Altogether, the interacting formalism outlined in this Letter constitutes a large step in bringing theoretical studies up to speed with ability of experimentalists to measure AR lifetimes and, in general, multiexciton dynamics. Our approach allows for direct comparisons and joint investigations between

theorists and experimentalists as it permits accurate theoretical calculations of AR lifetimes for experimentally relevant nanostructures of any dimensionality and composition. It should be noted that our framework assumes the excitons scatter coherently; thus, systems in which exciton diffusion is the rate limiting step are currently outside the scope of our approach. In future work we plan to apply our formalism to study AR in CdSe NPLs and extend it to also include exciton diffusion processes, to resolve another experimentally controversy where two different methods provide significantly different scaling behaviors in 2D NPLs.^{29,31}

Methods

A detailed derivation of the equations along with additional information and discussion on the implementation of the theory using the semi-empirical pseudopotential method, filter-diagonalization technique, Bethe-Salpeter equation, Fermi's golden rule in the AR lifetime calculations presented in this Letter and the procedure used to construct the CdSe QDs and NRs is also outlined. This material is available at <https://doi.org/>.

References

1. Klimov, V. I., Mikhailovsky, A. A., McBranch, D. W., Leatherdale, C. A. & Bawendi, M. G. Quantization of Multiparticle Auger Rates in Semiconductor Quantum Dots. *Science* **287**, 1011–1013 (2000).
2. Klimov, V. I. Multicarrier Interactions in Semiconductor Nanocrystals in Relation to the Phenomena of Auger Recombination and Carrier Multiplication. *Annu. Rev. Condens. Matter Phys.* **5**, 285–316 (2014).

3. Colvin, V. L., Schlamp, M. C. & Alivisatos, A. P. Light-emitting diodes made from cadmium selenide nanocrystals and a semiconducting polymer. *Nature* **370**, 354–357 (1994).
4. Imamoglu, A. *et al.* Quantum correlation among photons from a single quantum dot at room temperature. *Nature* **406**, 968–970 (2000).
5. Pietryga, J. M., Zhuravlev, K. K., Whitehead, M., Klimov, V. I. & Schaller, R. D. Evidence for barrierless auger recombination in PbSe nanocrystals: A pressure-dependent study of transient optical absorption. *Phys. Rev. Lett.* **101**, 217401 (2008).
6. Bae, W. K. *et al.* Controlled alloying of the core-shell interface in CdSe/CdS quantum dots for suppression of auger recombination. *ACS Nano* **7**, 3411–3419 (2013).
7. Fathpour, S. *et al.* The role of Auger recombination in the temperature-dependent output characteristics ($T_0 = \infty$) of p-doped 1.3 μm quantum dot lasers. *Appl. Phys. Lett.* **85**, 5164–5166 (2004).
8. Sukhovatkin, V., Hinds, S., Brzozowski, L. & Sargent, E. H. Colloidal quantum-dot photodetectors exploiting multiexciton generation. *Science* **324**, 1542–1544 (2009).
9. Nair, G., Zhao, J. & Bawendi, M. G. Biexciton quantum yield of single semiconductor nanocrystals from photon statistics. *Nano Lett.* **11**, 1136–1140 (2011).
10. Ben-Shahar, Y. *et al.* Charge carrier dynamics in photocatalytic hybrid semiconductor-metal nanorods: crossover from Auger recombination to charge transfer. *Nano Lett.* **18**, 5211–5216 (2018).
11. Robel, I., Gresback, R., Kortshagen, U., Schaller, R. D. & Klimov, V. I. Universal size-dependent trend in auger recombination in direct-gap and indirect-gap semiconductor nanocrystals. *Phys. Rev. Lett.* **102**, 177404 (2009).

12. García-Santamaría, F. *et al.* Suppressed auger recombination in "Giant" nanocrystals boosts optical gain performance. *Nano Lett.* **9**, 3482–3488 (2009).
13. Pijpers, J. J. H., Milder, M. T. W., Delerue, C. & Bonn, M. (Multi)exciton Dynamics and Exciton Polarizability in Colloidal InAs Quantum Dots. *J. Phys. Chem. C.* **114**, 6318–6324 (2010).
14. Chepic, D. I. *et al.* Auger ionization of semiconductor quantum drops in a glass matrix. *J. Lumin.* **47**, 113–127 (1990).
15. Vaxenburg, R., Rodina, A., Shabaev, A., Lifshitz, E. & Efros, A. L. Nonradiative auger recombination in semiconductor nanocrystals. *Nano Lett.* **15**, 2092–2098 (2015).
16. Vaxenburg, R., Rodina, A., Lifshitz, E. & Efros, A. L. Biexciton Auger Recombination in CdSe/CdS Core/Shell Semiconductor Nanocrystals. *Nano Lett.* **16**, 2503–2511 (2016).
17. Cragg, G. E. & Efros, A. L. Suppression of auger processes in confined structures. *Nano Lett.* **10**, 313–317 (2010).
18. Zavelani-Rossi, M., Lupo, M. G., Tassone, F., Manna, L. & Lanzani, G. Suppression of biexciton auger recombination in CdSe/CdS Dot/rods: Role of the electronic structure in the carrier dynamics. *Nano Lett.* **10**, 3142–3150 (2010).
19. García-Santamaría, F. *et al.* Breakdown of volume scaling in auger recombination in CdSe/CdS heteronanocrystals: The role of the core-shell interface. *Nano Lett.* **11**, 687–693 (2011).
20. Park, Y. S., Bae, W. K., Padilha, L. A., Pietryga, J. M. & Klimov, V. I. Effect of the core/shell interface on auger recombination evaluated by single-quantum-dot spectroscopy. *Nano Lett.* **14**, 396–402 (2014).

21. Jain, A. *et al.* Atomistic Design of CdSe/CdS Core-Shell Quantum Dots with Suppressed Auger Recombination. *Nano Lett.* **16**, 6491–6496 (2016).
22. Jain, A., Voznyy, O., Korkusinski, M., Hawrylak, P. & Sargent, E. H. Ultrafast Carrier Trapping in Thick-Shell Colloidal Quantum Dots. *J. Phys. Chem. Lett.* **8**, 3179–3184 (2017).
23. Htoon, H., Hollingsworth, J. a., Dickerson, R. & Klimov, V. I. Effect of zero- to one-dimensional transformation on multiparticle Auger recombination in semiconductor quantum rods. *Phys. Rev. Lett.* **91**, 227401 (2003).
24. Taguchi, S., Saruyama, M., Teranishi, T. & Kanemitsu, Y. Quantized Auger recombination of biexcitons in CdSe nanorods studied by time-resolved photoluminescence and transient-absorption spectroscopy. *Phys. Rev. B* **83**, 155324 (2011).
25. Zhu, H. & Lian, T. Enhanced multiple exciton dissociation from CdSe quantum rods: The effect of nanocrystal shape. *J. Am. Chem. Soc.* **134**, 11289–11297 (2012).
26. Yang, J., Hyun, B. R., Basile, A. J. & Wise, F. W. Exciton relaxation in PbSe nanorods. *ACS Nano* **6**, 8120–8127 (2012).
27. Padilha, L. A. *et al.* Aspect Ratio Dependence of Auger Recombination and Carrier Multiplication in PbSe Nanorods. *Nano Lett.* **13**, 1092–1099 (2013).
28. Aerts, M. *et al.* Cooling and auger recombination of charges in PbSe nanorods: Crossover from cubic to bimolecular decay. *Nano Lett.* **13**, 4380–4386 (2013).
29. She, C. *et al.* Red, Yellow, Green, and Blue Amplified Spontaneous Emission and Lasing Using Colloidal CdSe Nanoplatelets. *ACS Nano* **9**, 9475–9485 (2015).

30. Stolle, C. J., Lu, X., Yu, Y., Schaller, R. D. & Korgel, B. A. Efficient Carrier Multiplication in Colloidal Silicon Nanorods. *Nano Lett.* **17**, 5580–5586 (2017).
31. Li, Q. & Lian, T. Area- and Thickness-Dependent Biexciton Auger Recombination in Colloidal CdSe Nanoplatelets: Breaking the Universal Volume Scaling Law. *Nano Lett.* **17**, 3152–3158 (2017).
32. Wang, F., Wu, Y., Hybertsen, M. S. & Heinz, T. F. Auger recombination of excitons in one-dimensional systems. *Phys. Rev. B* **73**, 245424 (2006).
33. Wang, L.-W., Califano, M., Zunger, A. & Franceschetti, A. Pseudopotential theory of Auger processes in CdSe quantum dots. *Phys. Rev. Lett.* **91**, 056404 (2003).
34. Korkusinski, M., Voznyy, O. & Hawrylak, P. Theory of highly excited semiconductor nanostructures including Auger coupling: Exciton-biexciton mixing in CdSe nanocrystals. *Phys. Rev. B* **84**, 155327 (2011).
35. Patton, B., Langbein, W. & Woggon, U. Trion, biexciton, and exciton dynamics in single self-assembled CdSe quantum dots. *Phys. Rev. B* **68**, 125316 (2003).
36. Balan, A. D. *et al.* Effect of Thermal Fluctuations on the Radiative Rate in Core/Shell Quantum Dots. *Nano Lett.* **17**, 1629–1636 (2017).
37. Refaely-Abramson, S., Da Jornada, F. H., Louie, S. G. & Neaton, J. B. Origins of Singlet Fission in Solid Pentacene from an ab initio Green's Function Approach. *Phys. Rev. Lett.* **119**, 267401 (2017).
38. Rohlfing, M. & Louie, S. G. Electron-hole excitations and optical spectra from first principles. *Phys. Rev. B* **62**, 4927–4944 (2000).
39. Eshet, H., Grünwald, M. & Rabani, E. The electronic structure of CdSe/CdS Core/shell seeded nanorods: Type-I or quasi-type-II? *Nano Lett.* **13**, 5880–5885 (2013).

40. Jasieniak, J., Califano, M. & Watkins, S. E. Size-dependent valence and conduction band-edge energies of semiconductor nanocrystals. *ACS Nano* **5**, 5888–5902 (2011).
41. Franceschetti, A. & Zunger, A. Direct pseudopotential calculation of exciton coulomb and exchange energies in semiconductor quantum dots. *Phys. Rev. Lett.* **78**, 915–918 (1997).
42. Wang, L. W. & Zunger, A. Electronic Structure Pseudopotential Calculations of Large (.apprx.1000 Atoms) Si Quantum Dots. *J. Phys. Chem.* **98**, 2158–2165 (1994).
43. Wang, L.-W. & Zunger, A. Pseudopotential calculations of nanoscale CdSe quantum dots. *Phys. Rev. B* **53**, 9579–9582 (1996).
44. Rabani, E., Hetenyi, B., Berne, B. J. & Brus, L. E. Electronic properties of CdSe nanocrystals in the absence and presence of a dielectric medium. *J. Chem. Phys.* **110**, 5355–5369 (1999).
45. Williamson, A. & Zunger, A. Pseudopotential study of electron-hole excitations in colloidal free-standing InAs quantum dots. *Phys. Rev. B* **61**, 1978–1991 (2000).
46. Wall, M. R. & Neuhauser, D. Extraction, through filter-diagonalization, of general quantum eigenvalues or classical normal mode frequencies from a small number of residues or a short-time segment of a signal. I. Theory and application to a quantum-dynamics model. *J. Chem. Phys.* **102**, 8011–8022 (1995).
47. Toledo, S. & Rabani, E. Verly large electronic structure calculations using an out-of-core filter-diagonalization method. *J. Comput. Phys.* **180**, 256–269 (2002).
48. Shabaev, A. & Efros, A. L. 1D exciton spectroscopy of semiconductor nanorods. *Nano Lett.* **4**, 1821–1825 (2004).

49. Rabani, E. & Baer, R. Theory of multiexciton generation in semiconductor nanocrystals. *Chem. Phys. Lett.* **496**, 227–235 (2010).
50. Baer, R. & Rabani, E. Expeditious stochastic calculation of multiexciton generation rates in semiconductor nanocrystals. *Nano Lett.* **12**, 2123–2128 (2012).
51. Cunningham, P. D. *et al.* Enhanced multiple exciton generation in quasi-one-dimensional semiconductors. *Nano Lett.* **11**, 3476–3481 (2011).
52. Sandberg, R. L. *et al.* Multiexciton dynamics in infrared-emitting colloidal nanostructures probed by a superconducting nanowire single-photon detector. *ACS Nano* **6**, 9532–9540 (2012).
53. Baer, R. & Rabani, E. Communication: Biexciton generation rates in CdSe nanorods are length independent. *J. Chem. Phys.* **138**, 051102 (2013).
54. Barzykin, A. V. & Tachiya, M. Stochastic models of carrier dynamics in single-walled carbon nanotubes. *Phys. Rev. B* **72**, 075425 (2005).
55. Ma, Y. Z., Valkunas, L., Dexheimer, S. L., Bachilo, S. M. & Fleming, G. R. Femtosecond spectroscopy of optical excitations in single-walled carbon nanotubes: Evidence for exciton-exciton annihilation. *Phys. Rev. Lett.* **94**, 157402 (2005).
56. Huang, L. & Krauss, T. D. Quantized bimolecular auger recombination of excitons in single-walled carbon nanotubes. *Phys. Rev. Lett.* **96**, 057407 (2006).
57. Wang, F., Dukovic, G., Brus, L. E. & Heinz, T. F. The Optical Resonances in Carbon. *Science* **308**, 838–841 (2005).

58. Pal, S., Casanova, D. & Prezhd, O. V. Effect of Aspect Ratio on Multiparticle Auger Recombination in Single-Walled Carbon Nanotubes: Time Domain Atomistic Simulation. *Nano Lett.* **18**, 58–63 (2018).

Supplementary Information is available for this paper at <https://doi.org/>.

Acknowledgements The authors thank Mr. Devan Skubitz for preliminary tests of the developed code and Dr. Felipe H. Jornada and Prof. Steven G. Louie for stimulating discussions. This research was supported by the University of California Lab Fee Research Program (Grant LFR-17-477237) and used resources of the National Energy Research Scientific Computing Center (NERSC), a U.S. Department of Energy Office of Science User Facility operated under Contract No. DE-AC02-05CH11231.

Author Contributions J.P.P and E.R. developed the theoretical framework, computer code, performed the calculations and co-wrote the paper.

Competing Interests The authors declare that they have no competing financial interests.

Correspondence Correspondence and requests for materials should be addressed to J.P.P. (email: jphilbin@berkeley.edu) or to E.R. (email: eran.rabani@berkeley.edu).

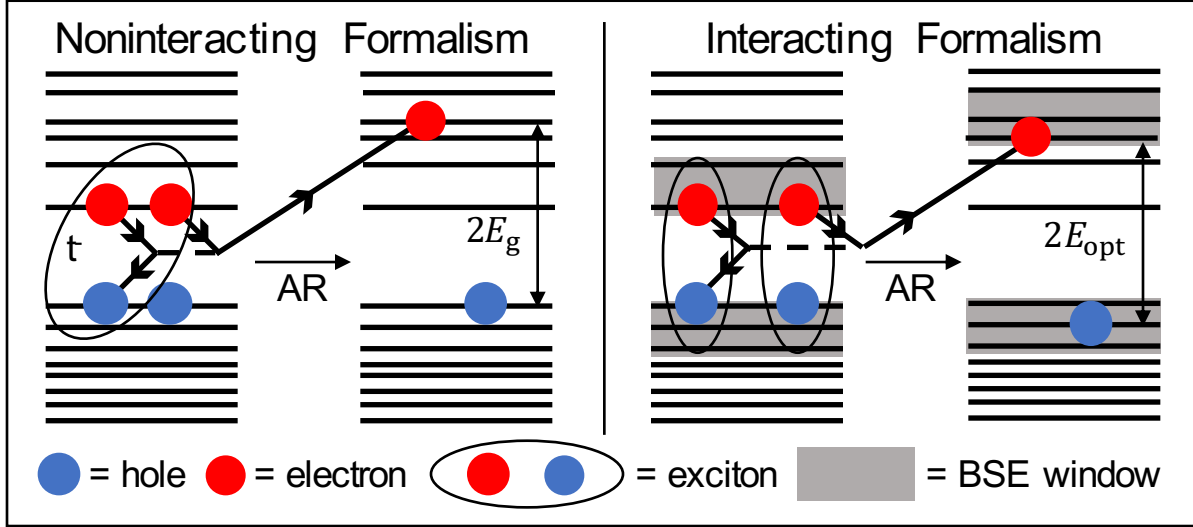


Figure 1: Pictorial representations are shown for the electron channel of an Auger recombination (AR) event in the noninteracting (left) and interacting (right) formalisms. The black horizontal lines represent the discrete quasiparticle states of the semiconductor nanostructures. The gray box in the interacting formalism represents the fact that the excitons (correlated electron–hole pairs) are a linear combination of the quasiparticle states within the box that were included in the BSE. E_g is the fundamental gap and E_{opt} is the optical gap. $|B\rangle^{(0)}$ is the initial state in the noninteracting formalism (note that one of the holes is a spectator and the AR process describes a negative trion, t^- , decaying to an excited quasidelectron state). $|B\rangle$ is the initial state in the interacting formalism composed of two excitons and all 4 particles are involved in the AR process. The final states in both formalisms are given by $|S\rangle^{(0)}$. The dashed line represents the Coulomb interaction.

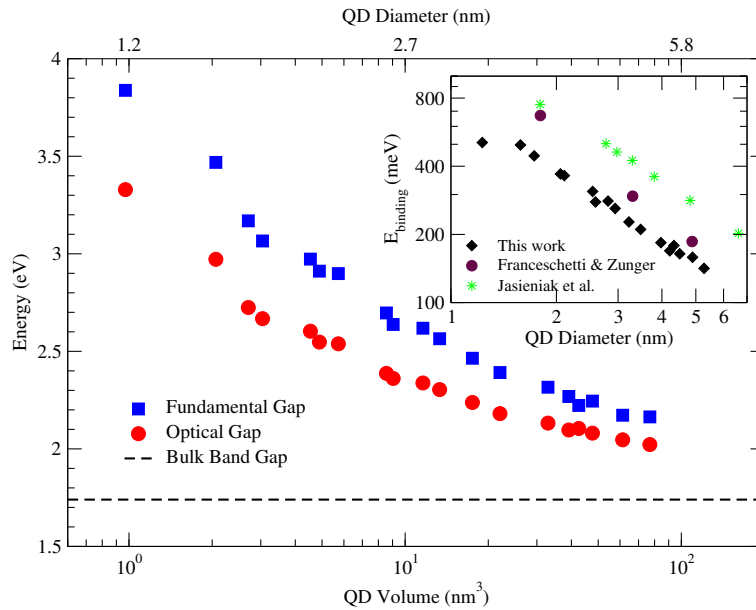


Figure 2: Energy gaps (in eV) for the seventeen CdSe QDs. The fundamental gap is shown in blue solid squares and the optical gap is shown in red solid circles. The inset shows the exciton binding energy (the energy difference between the fundamental and optical gaps) which ranges from ~ 500 meV for the smallest QDs to ~ 150 meV for the largest QDs studied here. For comparison, we also show the measured exciton binding energy (green stars, Ref. 40) and calculations based on a semi-empirical pseudopotential model using a perturbative scheme (maroon circles, Ref. 41).

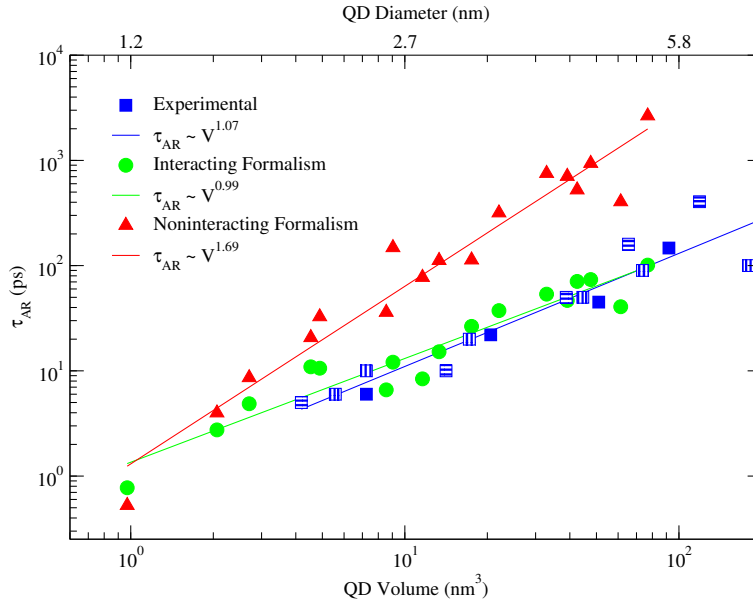


Figure 3: AR lifetimes, τ_{AR} , for CdSe QDs as a function of the volume of the QD. Good agreement is observed between the interacting formalism (green circles) and experimental (blue squares: solid,¹ vertical lines²³ and horizontal lines²⁴) AR lifetimes for all sizes. On the other hand, the noninteracting formalism (red triangles) deviates from the experimental values for QD volumes $> 10 \text{ nm}^3$. Power law fits, $\tau_{AR} = a \times V^b$, are also shown for each of the three sets of AR lifetimes.

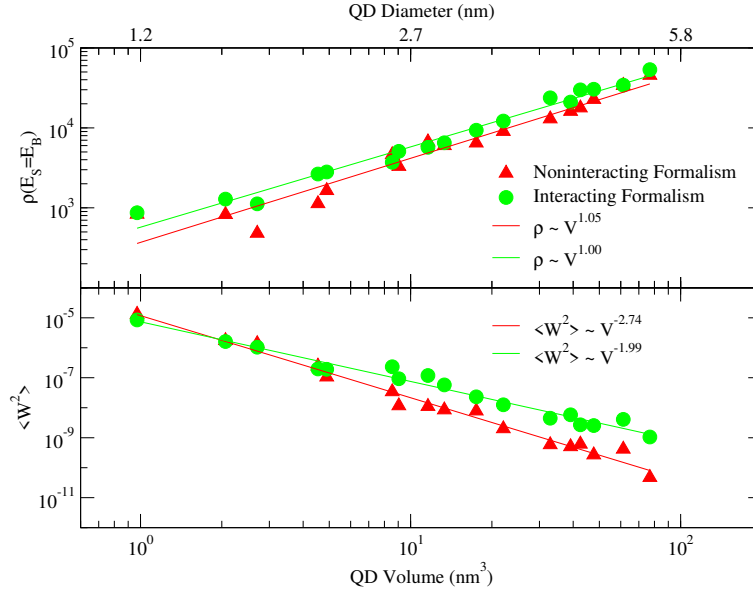


Figure 4: The top half shows the density of states at the energy of the hot electron and holes satisfying energy conservation for CdSe QDs as a function of the volume of the QD. The hot electrons (holes) have energies approximately E_g above (below) the HOMO (LUMO) in the noninteracting case and in the interacting formalism the hot electrons (holes) have energies approximately E_{opt} above (below) the HOMO (LUMO). The bottom half shows the average of the Coulomb couplings, $\langle W^2 \rangle$, squared to the final states. The noninteracting formalism results are shown as red triangles and the interacting formalism results are shown as green circles. Power law fits, $f(V) = a \times V^b$, are also shown for all sets.

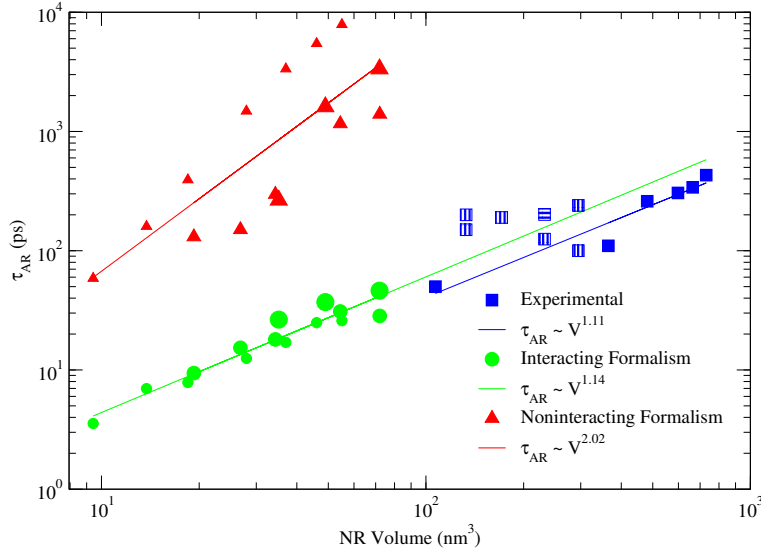


Figure 5: Auger recombination lifetimes for CdSe NRs as a function of the volume of the NRs predicted by the interacting (green circles), the noninteracting (red triangles) formalisms along with experimentally measured (blue squares: solid ²³, vertical ²⁴ and horizontal ²⁵ lines) AR lifetimes. The three different sizes used correspond to the three different diameters (1.53 nm, 2.14 nm and 2.89 nm) studied computationally. Power law fits, $\tau_{AR} = a \times V^b$, are also shown for each of the three sets of AR lifetimes.

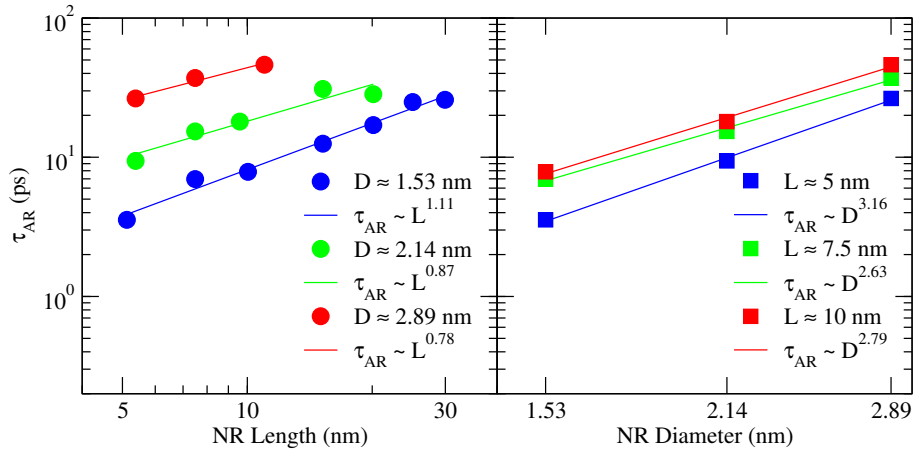


Figure 6: Interacting formalism based Auger recombination lifetimes for CdSe NRs as a function of the length (left) and diameter (right) of the NR. Power law fits, $\tau_{AR} = a \times D^b$ and $\tau_{AR} = a \times L^b$, are also shown for each NR set.